Graphene edge chemistry and membrane formation with supramolecular approaches using Pt(II)-terpyridine molecular tweezers

Jiao, A.

CHAPTER 7

Summary and outlook

7.1 Summary

DNA sequencing technology has evolved tremendously over the past five decades, from the Sanger sequencing to Illumina's sequencing-by-synthesis to nanopore sequencing technology pioneered by Oxford Nanopore Technologies (ONT). While these efforts have made DNA sequencing widely accessible, the technology continues to evolve. State-of-the-art biological nanopores are chemically well-defined and can be engineered to achieve appropriate DNA translocation speeds. However, their compatibility with protein sequencing is limited due to their poor stability under the extreme buffer conditions required to denature analyte proteins, such as high concentrations of urea, guanidinium chloride, or SDS.[1] Solid-state nanopore technology can provide a more versatile platform in the field of single-molecule sequencing. Graphene nanopores, in particular, have gained much attention thanks to their stability and one-atom thickness, which enables ultimate spatial resolution for sequencing technology.[2] However, the development of well-defined graphene nanopores is hindered by complex fabrication and characterization challenges, emphasizing the need for more chemically precise methods. While modification of graphene edges through covalent functionalization methods, such as diazonium chemistry, is often accompanied by side reactions on the basal plane,[3] non-covalent functionalization methods are non-invasive and preserve the mechanical and electrical properties of pristine graphene. To this end, this thesis explores possibilities of graphene nanopore functionalization using molecular tweezers.

Chapter 2 starts with examining the influence of the solvent on host-guest interactions between Pt(II)-terpyridine molecular tweezer **1** and coronene (Figure 7.1). The binding affinity of tweezer **1** to coronene was studied using titration experiments in single and binary mixtures of five different organic solvents: chloroform ($CHCl_3$), acetone, dimethylformamide (DMF), acetonitrile (MeCN) and methanol (MeOH). In single-solvent systems, the Gibbs free energy of association (ΔG^0_a) for tweezers-coronene complexation became more negative with increasing solvent polarity (expressed in $E_T(30)$). This increased binding affinity with increasing solvent polarity is attributed to solvophobic effects. In multi-solvent systems, however, the values of ΔG^0_a vs. $E_T(30)$ could not be described by the same single linear correlation. Instead, two linear correlations (one positive and one negative) were observed when plotting the values of ΔG^0_a vs. solvent fraction, resulting in a volcano plot for each solvent mixture. These plots describe the multi-faceted impact of introducing a secondary solvent, which can promote solubilization or generate solvophobic effects depending on the interplay between existing solvent-

solvent, solvent-solute, and solute-solute interactions: when a secondary solvent is introduced to an existing solvent medium, additional types of non-covalent interactions provided by the secondary solvent can stabilize individual host and guest components in solution, leading to a reduction in the observed binding affinity. The binding affinity reaches a minimum at a certain binary solvent composition, and deviating from this composition increases the binding affinity either through increasing the solvent-solvent interactions (when shifting the solvent composition towards the more polar solvent) or decreasing the solvent-solute interactions (when shifting the solvent composition towards the less polar solvent).

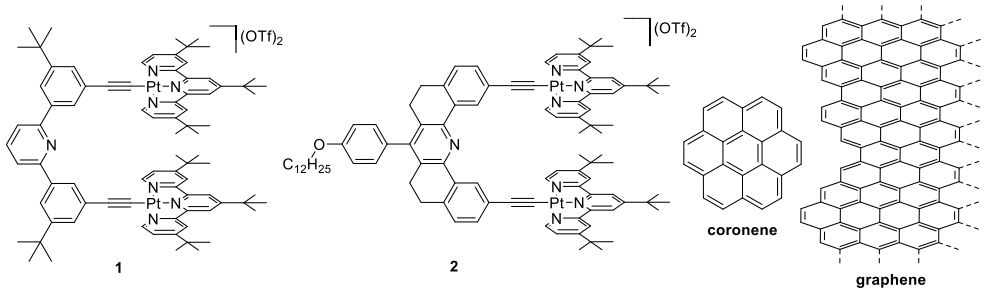

Figure 7.1 Structures of the primary molecular tweezers (host) and PAHs (their guests) reported in this thesis. Tweezer **1** contains a flexible 2,6-diphenylpyridine backbone connecting two Pt(II)-terpyridine arms. Tweezer **2** contains a rigid 5,6,8,9-tetrahydrodibenzo[c,h]acridine backbone connecting the same two Pt(II)-terpyridine arms. Coronene is one of the largest polycyclic aromatic hydrocarbons that remain soluble at millimolar concentrations. Coronene serves as a model for graphene, which is a two-dimensional material composed of sp^2-hybridized carbon atoms arranged in a hexagonal lattice.

Chapter 3 describes the importance of the backbone in molecular tweezers and the synthesis of a novel, preorganized Pt(II)-terpyridine molecular tweezer **2** (Figure 7.1) to improve upon the initial flexible molecular tweezer **1**. The design involves a rigid 5,6,8,9-tetrahydrodibenzo[c,h]acridine backbone instead of a flexible 2,6-diphenylpyridine backbone, accompanied by a dodecyl chain to bestow excellent solubility in organic solvents (Figure 7.1). The Gibbs free energy of association (ΔG^0_a), enthalpy of association (ΔH^0_a), and entropy of association (ΔS^0_a) of both tweezers **1** and **2** to coronene were investigated over a temperature range of 10–40 °C. These results provided insights into the binding properties, revealing more negative values of ΔG^0_a with decreasing temperature for both tweezers, demonstrating that the host-guest complexation reaction is exothermic. Moreover, both tweezers exhibited similar values for ΔH^0_a, as expected, since the arms

remained the same. Finally, negative values for ΔS^0_a were observed for both tweezers, which can be attributed to an entropic penalty associated with the complexation. This entropic penalty was smaller for the preorganized tweezers than for the flexible tweezers. Overall, introducing preorganization in the molecular tweezers increased the binding affinity by ~2.7 kJ mol^{-1}.

Chapter 4 describes the importance of size, geometry and edge functionality of the guest by studying the binding of Pt(II)-terpyridine molecular tweezer **2** to seven planar polycyclic aromatic hydrocarbons (PAHs) of varying sizes (4 – 8 fused rings), six non-planar PAHs, and one nitrogenated-PAH. Titration experiments revealed that the size of the PAH increases the π surface area available for π-π stacking with molecular tweezers, as ΔG^0_a values became more negative with increasing number of double bonds and topological resonance energy (TRE) in the PAH. The geometry of the PAH imposes a preferential orientation within the tweezers' cavity to maximize the π-π stacking overlap, which can be elucidated from a combination of Nuclear Overhauser Effect Spectroscopy (NOESY) and the magnitude of spectroscopic shifts obtained from the titration experiments. These techniques were particularly useful for understanding the influence of nitrogen substitution on the binding: triazacoronene, which is a coronene analogue in which three carbon atoms on the edge are substituted with nitrogen atoms, exhibited reduced binding affinity because of the reduced size of the π-electron cloud and unfavorable orientations in the tweezers' cavity. Finally, the planarity of the PAH dictates its recognition by molecular tweezers, revealing that the cavity of the Pt(II)-terpyridine molecular tweezers can only accommodate planar PAHs.

In Chapter 5, a practical and straightforward protocol for single or multiple graphene nanopore fabrication using automated controlled breakdown in NaCl solutions is established. Software parameters such as breakdown threshold and fabrication voltages were optimized to minimize program failures to facilitate efficient graphene nanopore fabrication. Various sample parameters, such as the freestanding graphene area and the presence of sodium dodecyl sulfate (SDS) in electrolyte solutions, were investigated to assess their influence on fabrication voltages, pore stability, $1/f$ noise, and multiporosity. Smaller freestanding areas of graphene required higher fabrication voltages, which can be explained by a lower number of defect sites necessary for pore formation. In turn, smaller freestanding graphene areas resulted in improved pore stability and reduced $1/f$ noise. Adding micromolar SDS to the electrolyte solution to enhance wetting could improve the controlled breakdown efficacy and nanopore stability. Finally, hydrophilic coatings were applied to characterize the multiporosity and individual pore sizes, which would otherwise

require complex techniques such as transmission electron microscopy (TEM). The reported fabrication and characterization methods serve as a basis for future optimization of graphene nanopore fabrication by automated controlled breakdown.

Chapter 6 diverges slightly from the previous chapters and describes bottom-up fabrication of 2D materials using π-π stacking interactions. The Langmuir-Blodgett technique provides a versatile platform for 2D material fabrication, as the obtained films on the water surface can be easily deposited onto the substrate of choice. By exploiting steric and π-π stacking interactions, borazine-based aromatic gear-shaped structures can self-assemble into organized thin films on a water surface. The deposition of the borazine precursors was optimized to limit aggregation of these hydrophobic compounds by minimizing the concentration and carefully controlling the deposition process. The resulting Langmuir films exhibited bimolecular thickness and freestanding ability enabled by intermolecular π-π stacking between anthracene groups, as confirmed by atomic force microscopy, fluorescence spectroscopy and scanning electron microscopy. This work highlights the critical role of π-π stacking interactions in the development of 2D materials, particularly readily transferrable thin films.

7.2 Outlook

This thesis mainly focused on the interactions between molecular tweezers and PAHs, examining how the host, guest and solvent components can be manipulated to control the binding of tweezers to aromatic substrates. This section converges on the results in the thesis to discuss the next step of implementing molecular tweezers to fabricate non-covalently functionalized graphene nanopores. Additionally, some preliminary results are presented to lay the groundwork for further investigation.

7.2.1 Rational optimization of tweezer-graphene interactions

Strong and selective tweezer-graphene interactions are crucial for the applicability of non-covalently functionalized graphene nanopore devices for DNA sequencing. First, high binding affinities allow adequate functionalization without the need for highly concentrated tweezer solutions, which is particularly important if the tweezer is poorly soluble. Second, sufficient device stability is necessary to allow continuous conductance measurements for the sequencing of long biopolymers and biopolymer fragments, *e.g.* the tweezer is not removed from the edge during said measurement. Finally, if the tweezers do detach from the graphene, these free tweezers may interfere with the measurement if the target biopolymer contains aromatic moieties, such as DNA. In the case of DNA, since nucleobases consist of only one or two fused aromatic rings, the binding of Pt(II)-terpyridine tweezers to such small aromatic moieties is expected to not outcompete that of the much larger graphene sheet (see Chapter 4). Still, considering the large number of nucleobases per DNA strand, any interference due to unintentional non-covalent interactions between free tweezers and DNA may prevent the device to run properly. Therefore, for DNA sequencing applications the tweezer must strongly and selectively bind to graphene.

In Chapter 3, it was demonstrated that tweezer **2** binds stronger to coronene than tweezer **1**, making tweezer **2** the better candidate for graphene edge functionalization (Figure 7.2). In Chapter 2, it was demonstrated that the binding of molecular tweezer **1** to coronene is highest in MeOH compared to $CHCl_3$, acetone, DMF or MeCN due to solvophobic effects. While the binding between tweezer **2** to PAHs has not been characterized in different solvents, we hypothesize the binding between tweezer **2** and PAHs is similarly driven by solvophobic effects as the binding of tweezer **1** and coronene. Therefore, to initiate strong binding of tweezer **2** to graphene, submerging graphene in a methanolic solution of tweezer **2** and rinsing the graphene with MeOH (which is, for example, more polar than acetone) would be the safest choice to retain graphene edge functionalization. Since the binding is strongly solvophobic, the binding could be even stronger in an aqueous environment. However, since the

tweezer is poorly soluble in aqueous solutions, functionalization in aqueous solutions would not necessarily be better than using more concentrated methanolic solutions. Nevertheless, we can expect the tweezer to remain bound to the graphene when switching from organic to aqueous solutions due to stronger solvophobic effects in water compared to lower polarity solvents such as methanol or acetone, which is important considering DNA sequencing is generally performed in aqueous solutions. Alternatively, the tweezers' solubility in water can be increased by changing the chemical structure, for example, adding polyethylene glycol chains to the backbone (Scheme 7.1).

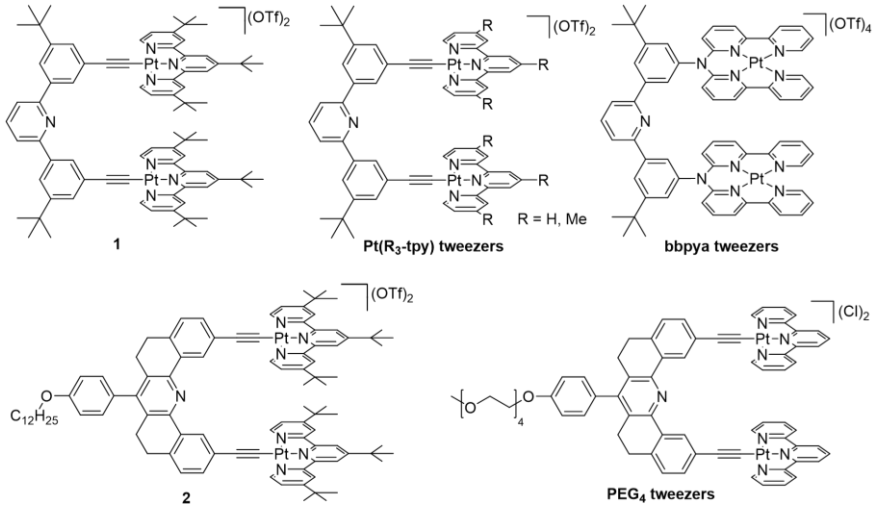

Figure 7.2 Structures and analogues of molecular tweezers 1 and 2. Pt(R_3-tpy) tweezers are less bulky analogues of **1**. Bbpya tweezers are analogues of **1** with more positively charged Pt atoms and increased stability. PEG_4 tweezers are water-soluble analogues of **2**.

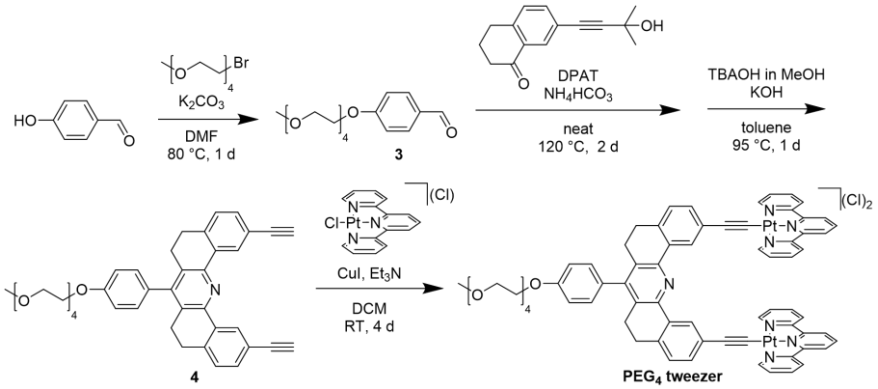

Scheme 7.1 Proposed reaction scheme for an analogue of tweezer 2 with increased water solubility (PEG_4 tweezer). DPAT = diphenylammonium triflate. TBAOH = *tert*-butylammonium hydroxide. RT = room temperature.

The synthesis route of tweezer **2** in Chapter 3 can be easily adapted to enable the preparation of derivatives with higher water solubility, such as the PEG_4 tweezers (Scheme 7.1). First, the hydrophilic tail **3** can be prepared by alkylation of benzaldehyde with the commercially available m-PEG_4-bromide. Second, Hanzsch pyridine synthesis of **3** with hydroxymethylbutynyl-3,4-dihydronaphthalenone (prepared in Chapter 3), followed by deprotection of the acetylene moieties, can afford backbone **4** equipped with a hydrophilic tail. Finally, backbone **4** can be coupled to the [Pt(tpy)Cl]Cl complex to form the arms and to afford the PEG_4 tweezer as the water-soluble analogue of tweezer **2**. Besides containing the hydrophilic PEG_4 tail, the proposed PEG_4 tweezer also features terpyridine ligands without hydrophobic *tert*-butyl (tBu) groups on the arms, as well as chloride counterions instead of triflate to improve water solubility.

Next to changing the backbone of the tweezers, which has been demonstrated to affect the entropy and subsequently the binding affinity of the tweezers in Chapter 3, the chemical structure of the "arms" can also be changed. The arms of the tweezers discussed in this thesis now contain several *tert*-butyl (tBu) groups on the terpyridine (tpy) ligand, which offers increased solubility in organic solvents and can sterically hinder self-association of the tweezers.[4] We hypothesize that changing the Pt(tBu_3-tpy) arms to less bulky alternatives like Pt(Me_3-tpy) or Pt(tpy) moieties may decrease steric hindrance with the guest and therefore increase the tweezers' binding affinity (Figure 7.2). Alternatively, the arms can be changed to employ other ligands such as N,N-bis(2–2′-bipyrid-6-yl)amine (bbpya) (Figure 7.2). These tetradentate ligands can offer greater stability than monodentate ligands such as acetylides. Additionally, neutral bbpya ligands can be used instead of negatively charged acetylide ligands to achieve a higher positive charge on the Pt atoms in the molecular tweezers. This increase in charge can offer increased charge transfer, donor-acceptor, and cation-π interactions with PAHs.

Unfortunately, in contrast to tweezers **1** and **2** containing bulky Pt(tBu_3-tpy) arms, the solubility of molecular tweezers with less bulky Pt(tpy) or Pt(Me_3-tpy) arms was dramatically reduced, which likely originated from high degrees of self-association and possible supramolecular polymerization when the tBu groups were not present on the arms (Figure 7.3). Consequently, the characterization of these tweezers with less bulky Pt(Me_3-tpy) arms was complicated, and purification using silica column chromatography, size exclusion chromatography and crystallization was unsuccessful. In the future, alternative techniques such as alumina or reverse-phase column chromatography may be more effective.

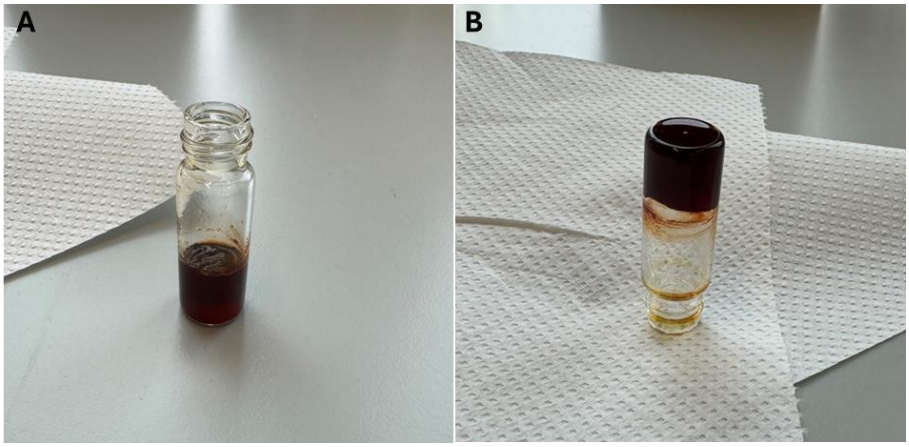

Figure 7.3 Gel formation of Pt(Me_3-tpy) tweezers in a mixture of dimethyl formamide (DMF) and diethyl ether (Et_2O). (A) After allowing a solution of crude Pt(Me_3-tpy) tweezers in DMF and Et_2O to evaporate in air under ambient conditions, a dark red gel was obtained. (B) The formed gel exhibited sufficient mechanical stability to retain its shape when the vial was inverted.

7.2.2 Tweezers interactions with the basal plane

From an organic chemist's perspective, non-covalent interaction between molecular tweezers and graphene might seem to be a simple, dynamic 1:1 equilibrium, where the binding can be reversed by changing the concentration of the interacting species. However, when working with 2D materials like graphene, this classical view of non-covalent interactions becomes insufficient. Graphene is notorious for surface contamination problems,[5] and many molecules such as polymer residues from graphene transfer methods[6] and airborne hydrocarbons[7,8] can non-covalently adhere to the graphene surface. These non-covalently bound contaminants often exhibit surprisingly strong binding and cannot be completely removed by rinsing in any amount of solvent, suggesting that the classical notion of reversible dynamic equilibrium does not fully apply to these surfaces. The observation of such irreversible binding phenomena suggests that non-covalent functionalization of graphene edges with molecular tweezers may exhibit similarly high stability. When introducing the molecular tweezers to graphene, the tweezers can interact with both the edge and the basal plane of graphene. Note that the structure of flexible tweezer **1** allows accommodation of a planar structure through bond rotations in the 2,6-diphenylpyridine backbone. Therefore, by employing a rigid backbone as described in Chapter 3, the propensity of rigid tweezer **2** binding to the basal plane could be decreased. In other words, by preventing full planarization of the molecular tweezer, the tweezers' selectivity may be increased towards the graphene edges.

To investigate whether the tweezers bind to the basal plane of graphene, X-ray photoelectron spectroscopy (XPS) and transmission electron microscopy energy dispersive X-ray spectroscopy (TEM-EDX) experiments were performed. For XPS, graphene samples were prepared on Si/SiO_2 wafer *via* the PMMA-assisted transfer method described in Chapter 5. The graphene samples were either dip-coated in pure $CHCl_3$ (negative control), a solution of tweezer **1** (1.0 mM) in $CHCl_3$ (positive control), or a solution of tweezer **1** (1.0 mM) in $CHCl_3$ followed by a single washing step (dipping in 10 mL $CHCl_3$ for 10 s), and dried in air. XPS measurements were performed in collaboration with Prof. dr. Jan Philipp Hoffmann, Dr. Clément Maheu and Dr. Hikmet Sezen. A negligible amount of N and F content was observed for the graphene sample dip-coated in pure $CHCl_3$ (red traces in Figure 7.4). An increase in N and F content was observed for the graphene sample dip-coated in a solution of tweezer **1** in $CHCl_3$ (1.0 mM) without washing (green traces in Figure 7.4). These signals decreased significantly after the $CHCl_3$ washing step, suggesting that most of the tweezers can be removed from the basal plane (blue traces in Figure 7.4). Small signals were still observed after washing, suggesting that a fraction of tweezer **1** remained bound to the graphene after a single $CHCl_3$ washing step.

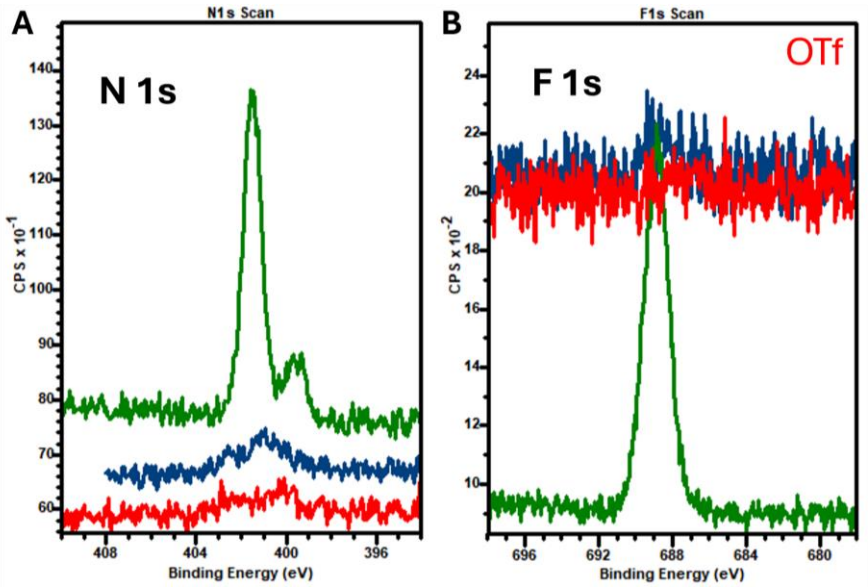

Figure 7.4 Studying the interactions of molecular tweezer 1 to the basal plane of graphene by XPS. Graphene samples transferred onto Si/SiO_2 substrates were either dip-coated in pure $CHCl_3$ (negative control, red traces), a solution of tweezer **1** (1.0 mM) in $CHCl_3$ (positive control, green traces), or a solution of tweezer **1** (1.0 mM) in $CHCl_3$ followed by dipping in 10 mL $CHCl_3$ for 10 s (blue traces). (A) The N 1s content in the three different samples. (B) The F 1s content in the three different samples.

To investigate the interaction between tweezers and graphene by TEM, first graphene samples were prepared in collaboration with Thomas Kock on Au TEM grids covered with Quantifoil® containing 1.2 µm diameter holes spaced 1.3 µm apart (R 1.2/1.3) *via* the direct transfer method from Regan et al.[9] Similar to the XPS experiments, the graphene samples were either dip-coated in pure $CHCl_3$, a solution of tweezer **1** (1.0 mM) in $CHCl_3$, or a solution of tweezer **1** (1.0 mM) in $CHCl_3$ followed by dipping in 10 mL $CHCl_3$ for 10 s, and dried in air. TEM measurements were performed in collaboration with Thomas Kock and Nemo Andrea. Negligible amount of surface contamination was observed for the graphene sample dip-coated in pure $CHCl_3$ (Figure 7.5A). Circular structures were observed for the graphene sample dip-coated in a solution of tweezer **1** in $CHCl_3$ (1.0 mM) without washing, which may be concentrated areas of tweezer **1** after evaporation of the solvent (Figure 7.5B). After dipping in 10 mL $CHCl_3$ for 10 s, large aggregates were removed (Figure 7.5C). When performing TEM-EDX experiments to visualize the Pt signals in tweezer **1**, these signals were hidden beneath large Au signals originating from the Au TEM grid (Figure 7.5D). Even though the results were not conclusive, these experiments suggest that small amounts of tweezer **1** can bind to the basal plane of graphene. In the future, TEM experiments should be repeated on Cu TEM grids to avoid overlap with the Pt signals during TEM-EDX experiments. Also, to investigate whether the increased rigidity can increase the edge selectivity of the tweezers, these experiments should be repeated with the rigid molecular tweezer **2**.

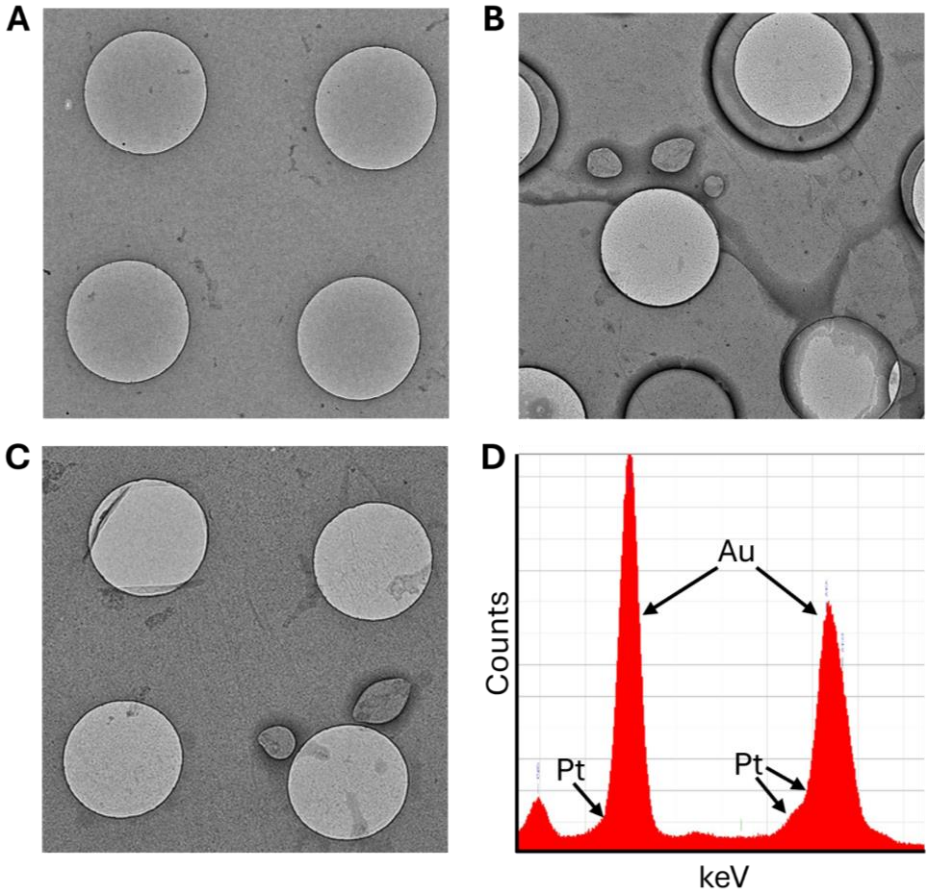

Figure 7.5 Studying the interactions of molecular tweezer 1 to the basal plane of graphene on Au/Quantifoil® (R 1.2/1.3) TEM grids by TEM-EDX. (A) TEM image of a graphene sample dipped in pure $CHCl_3$. (B) TEM image of a graphene sample dip-coated in a solution of tweezer **1** (1.0 mM) in $CHCl_3$. (C) TEM image of graphene sample dip-coated in a solution of tweezer **1** (1.0 mM) in $CHCl_3$ followed by dipping in 10 mL $CHCl_3$ for 10 s. (D) TEM-EDX spectrum of measured on the sample in panel C.

7.2.3 Tweezer interactions with the edge

The most interesting yet challenging aspect of this thesis lies in characterizing the interaction between the tweezers and the graphene edge. Several questions naturally arise: how does the chemical nature of the edge influence the binding? How can one effectively characterize the edge, which constitutes only a very small fraction of a graphene sample? Is the interaction between molecular tweezers and graphene stable or reversible? Many intriguing questions remain open for future exploration, and the research undertaken in this thesis has yielded valuable insights for future studies.

The chemical nature of the edge, including zigzag, armchair, nitrogenated and oxidized, can influence its interaction with molecular tweezers. Building on the results from Chapter 4, we hypothesize that zigzag and armchair edges do not influence the binding affinity of the tweezer directly. However, these structures can affect the chemical stability of the edge. For example, zigzag edges are generally more reactive and can be oxidized in the presence of air.[10,11] Moreover, in Chapter 4, it was demonstrated that edge heteroatoms can reduce the binding of molecular tweezers. Therefore, it is possible to alter the chemical structure of the graphene edge to manipulate the binding interactions. For example, introducing hydrogen-bond donors on the substrate can introduce hydrogen-bonding interactions with the central pyridine in the backbone of the molecular tweezers.[12,13] From this perspective, introducing carboxylic acids at the graphene edge could be a strategy to strengthen the binding with tweezers **1** and **2**, which contain a central pyridine in the backbone.

The intrinsic difficulty of characterizing graphene edges stems from their scarcity relative to the basal plane. Spectroscopic approaches, including Raman and XPS, can provide indirect characterization of graphene, however, the spatial resolution is insufficient to properly distinguish the edge from the basal plane. Microscopy methods such as high-resolution TEM or STM can provide direct visualization of the edges, however, the practicality of these methods is limited by demanding sample preparation and scalability issues. Patch-clamp methods, such as nanopore conductance experiments, are scalable and provide information specific to the structure around the graphene edges. Although the technique requires further optimization regarding scalable single-pore fabrication, nanopore stability and noise reduction, the intrinsic ability to differentiate the edge from the basal plane makes this technique a promising platform for future research.

To investigate whether the binding between molecular tweezers and graphene is reversible, the nanopore platform was used to monitor the conductance through graphene nanopores before and after functionalization with molecular tweezers (Figure 7.6A). These graphene nanopores were fabricated and monitored together with Aylin Peri Ayaydin using the protocols described in Chapter 5. Five graphene nanopore samples were prepared *via* nucleation in 3.6 M NaCl + 10 mM HEPES (18.89 S m^{-1}, pH 8.0), followed by enlargement to a pore size of 5 – 10 nm in 1.0 M NaCl + 10 mM HEPES (7.76 S m^{-1}, pH 8.0). The conductance through each nanopore sample was measured at voltages between -100 mV to 100 mV in 1.0 M NaCl + 10 mM HEPES (7.76 S m^{-1}, pH 8.0) at three different stages: first after conditioning, then after incubation with a solution of tweezer **1** in MeOH (1.0 mM) for 5 min, and finally after rinsing with MeOH and water. Preliminary experiments demonstrated

that after incubating graphene nanopore samples with tweezer **1** in MeOH, their initial conductance before incubation (29.7 – 60.8 nS) decreased after incubation (18.6 – 34.1 nS) in four out of five samples (Figure 7.6B). These conductance values correspond to 37% – 80% of the original conductance values before tweezers functionalization, suggesting graphene edge functionalization with molecular tweezers in these samples might have been obtained. After rinsing these samples thoroughly with MeOH and water, an increase in conductance was observed (36.0 – 41.2 nS). These conductance values correspond to 79% – 121% of the original conductance values before the functionalization with tweezers molecules, suggesting that the molecular tweezer can be removed from the edge after rinsing with organic solvents. The large variance in the changes in conductance values may be due to variation in multiporosity between different graphene nanopore samples fabricated by CBD as demonstrated in Chapter 5. Future studies can focus on optimizing the CBD protocol for the reliable fabrication of single graphene nanopores and measuring the pore conductance after incubation with other molecular tweezers, such as tweezer **2**.

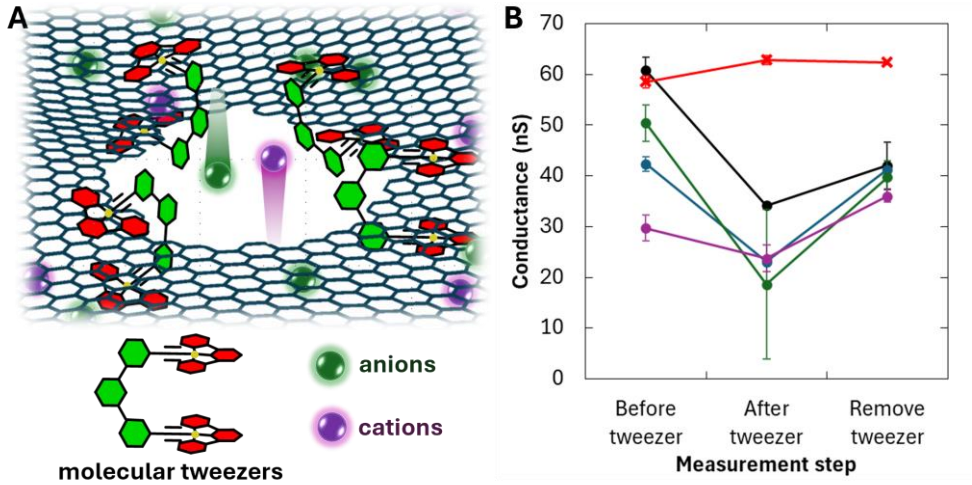

Figure 7.6 Molecular tweezers binding graphene nanopore edges. (A) Illustration of ions moving through graphene nanopores decorated with molecular tweezers on the edges. (B) Ion conductance measurements in 1.0 M NaCl + 10 mM HEPES (7.76 S m^{-1}, pH 8.0) through graphene nanopores before and after incubation with molecular tweezer **1** in MeOH (1.0 mM) for 5 min, and after removal of the tweezers after extensive rinsing with MeOH and water. Black, blue, green and purple dots indicate different graphene nanopore samples successfully functionalized with molecular tweezers. Red crosses indicate graphene samples that were unsuccessfully functionalized with molecular tweezers. Error bars represent standard deviations of 2 – 3 measurements with waiting times of 5 min between each measurement.

7.3 References

(1) Liu, M.; Li, J.; Tan, C. S. Unlocking the Power of Nanopores: Recent Advances in Biosensing Applications and Analog Front-End. *Biosensors* **2023**, *13* (6), 598. https://doi.org/10.3390/bios13060598.

(2) Can, B. S.; Blümel, N. V. V.; van Geest, E. P.; et al. A Perspective on Graphene Junctions for Recognition Tunneling. *Appl. Phys. Lett.* **2024**, *124* (21), 210501. https://doi.org/10.1063/5.0203315.

(3) Xiong, Z.; Gu, T.; Wang, X. Self-Assembled Multilayer Films of Sulfonated Graphene and Polystyrene-Based Diazonium Salt as Photo-Cross-Linkable Supercapacitor Electrodes. *Langmuir* **2014**, *30* (2), 522–532. https://doi.org/10.1021/la4037875.

(4) Doistau, B.; Tron, A.; Denisov, S. A.; et al. Terpy(Pt–Salphen)2 Switchable Luminescent Molecular Tweezers. *Chem. – Eur. J.* **2014**, *20* (48), 15799–15807. https://doi.org/10.1002/chem.201404064.

(5) Lin, L.; Zhang, J.; Su, H.; et al. Towards Super-Clean Graphene. *Nat. Commun.* **2019**, *10* (1), 1912. https://doi.org/10.1038/s41467-019-09565-4.

(6) Zhuang, B.; Li, S.; Li, S.; et al. Ways to Eliminate PMMA Residues on Graphene — — Superclean Graphene. *Carbon* **2021**, *173*, 609–636. https://doi.org/10.1016/j.carbon.2020.11.047.

(7) Temiryazev, A.; Frolov, A.; Temiryazeva, M. Atomic-Force Microscopy Study of Self-Assembled Atmospheric Contamination on Graphene and Graphite Surfaces. *Carbon* **2019**, *143*, 30–37. https://doi.org/10.1016/j.carbon.2018.10.094.

(8) Li, Z.; Wang, Y.; Kozbial, A.; et al. Effect of Airborne Contaminants on the Wettability of Supported Graphene and Graphite. *Nat. Mater.* **2013**, *12* (10), 925–931. https://doi.org/10.1038/nmat3709.

(9) Regan, W.; Alem, N.; Alemán, B.; et al. A Direct Transfer of Layer-Area Graphene. *Appl. Phys. Lett.* **2010**, *96* (11), 113102. https://doi.org/10.1063/1.3337091.

(10) Bellunato, A.; Arjmandi Tash, H.; Cesa, Y.; et al. Chemistry at the Edge of Graphene. *ChemPhysChem* **2016**, *17* (6), 785–801. https://doi.org/10.1002/cphc.201500926.

(11) Soldano, G. J.; Juarez, M. F.; Teo, B. W. T.; et al. Structure and Stability of Graphene Edges in O2 and H2 Environments from Ab Initio Thermodynamics. *Carbon* **2014**, *78*, 181–189. https://doi.org/10.1016/j.carbon.2014.06.070.

(12) Fu, T.; Han, Y.; Ao, L.; et al. Bis[Alkynylplatinum(II)] Terpyridine Molecular Tweezer/Guest Recognition Enhanced by Intermolecular Hydrogen Bonds: Phototriggered Complexation *via* the "Caging" Strategy. *Organometallics* **2016**, *35* (17), 2850–2853. https://doi.org/10.1021/acs.organomet.6b00429.

(13) Li, Z.; Han, Y.; Jin, F.; et al. Bis[Alkynylplatinum(II)] Terpyridine Molecular Tweezer with Conformationally-Rigid Spacer: Modulating the Binding Selectivity in a Three-Component Supramolecular Recognition System. *Dalton Trans.* **2016**, *45* (43), 17290–17295. https://doi.org/10.1039/C6DT03160A.